

Anharmonic Phonon Interactions at Interfaces and Contributions to Thermal Boundary Conductance

Patrick E. Hopkins¹
e-mail: pehopki@sandia.gov

John C. Duda

Engineering Sciences Center,
Sandia National Laboratories,
P.O. Box 5800,
Albuquerque, NM 87185-0346;
Department of Mechanical and Aerospace
Engineering,
University of Virginia,
Charlottesville, VA 22904-4746

Pamela M. Norris

Department of Mechanical and Aerospace
Engineering,
University of Virginia,
Charlottesville, VA 22904-4746

Continued reduction in characteristic dimensions in nanosystems has given rise to increasing importance of material interfaces on the overall system performance. With regard to thermal transport, this increases the need for a better fundamental understanding of the processes affecting interfacial thermal transport, as characterized by the thermal boundary conductance. When thermal boundary conductance is driven by phononic scattering events, accurate predictions of interfacial transport must account for anharmonic phononic coupling as this affects the thermal transmission. In this paper, a new model for phononic thermal boundary conductance is developed that takes into account anharmonic coupling, or inelastic scattering events, at the interface between two materials. Previous models for thermal boundary conductance are first reviewed, including the diffuse mismatch model, which only considers elastic phonon scattering events, and earlier attempts to account for inelastic phonon scattering, namely, the maximum transmission model and the higher harmonic inelastic model. A new model is derived, the anharmonic inelastic model, which provides a more physical consideration of the effects of inelastic scattering on thermal boundary conductance. This is accomplished by considering specific ranges of phonon frequency interactions and phonon number density conservation. Thus, this model considers the contributions of anharmonic, inelastically scattered phonons to thermal boundary conductance. This new anharmonic inelastic model shows improved agreement between the thermal boundary conductance predictions and experimental data at the Pb/diamond and Au/diamond interfaces due to its ability to account for the temperature dependent changing phonon population in diamond, which can couple anharmonically with multiple phonons in Pb and Au. We conclude by discussing phonon scattering selection rules at interfaces and the probability of occurrence of these higher order anharmonic interfacial phonon processes quantified in this work.
[DOI: 10.1115/1.4003549]

Keywords: thermal boundary conductance, Kapitza resistance, phonon interfacial scattering, elastic and inelastic scattering, harmonic and anharmonic processes

1 Introduction

Nanostructures are routinely fabricated with critical length scales on the order of carrier mean free paths. As a result, the need to understand the fundamental physical processes driving interfacial thermal transport is increasingly important if we are to understand, interpret, and predict thermophysical properties of such systems [1]. This is especially significant, as recent results show that Fourier's law breaks down even at length scales larger than the mean free path in nanostructures [2], thus causing h_K to play a larger role in thermal processes in low dimensional structures such as carbon nanotubes [3], superlattice films [4] and nanowires [5], and thin metal films [6–8]. The thermal boundary conductance h_K , the inverse of which is the Kapitza resistance R_K , creates a temperature drop across the interface that is related to the thermal flux by $h_K = 1/R_K = q_{\text{int}}/\Delta T$, where q_{int} is the interfacial heat flux between two materials and ΔT is the interfacial temperature drop [9].

The most commonly applied theoretical models for predicting

h_K are the acoustic mismatch model (AMM) [10] and the diffuse mismatch model (DMM) [11]. Accurate modeling of the thermal boundary conductance is a formidable task [12], as h_K is influenced by substrate surface roughness [13], quality of crystalline orientation [14], phonon mean free path [15], atomic diffusion [16], and intrinsic vibrational properties of the material (or “acoustic mismatch”) [7,8,17]. Several subsequent models have been proposed to explain discrepancies between model predictions and experimental measurements. Many of these models include other relevant physical properties or processes that the AMM and DMM do not take into account, including the use of an exact phonon dispersion [18] or measured phonon density of states [19] in the calculations, incorporating electron-phonon resistances at the interface [20], and accounting for multiple phonon scattering events around the interface [21–23]. All of these improvements help explain the discrepancies in the situation where the two materials comprising the interface are acoustically (or vibrationally) matched. However, attempts to explain the deviation between predictions and experimental data in the situation where the materials comprising the interface are acoustically mismatched have resulted in two conflicting theories over the past few decades.

Stoner and Maris [24] reported some of the first measurements of h_K at relatively high temperatures (50–300 K) on a range of acoustically mismatched solid-solid metal-dielectric interfaces. Their results showed that the DMM underpredicted the measured h_K by over an order of magnitude for interfaces that were heavily mismatched. These surprising results were theoretically explained

¹Corresponding author.

Contributed by the Heat Transfer Division of ASME for publication in the JOURNAL OF HEAT TRANSFER. Manuscript received June 16, 2010; final manuscript received January 12, 2011; published online March 9, 2011. Assoc. Editor: Patrick E. Phelan.

The United States Government retains, and by accepting the article for publication, the publisher acknowledges that the United States Government retains, a non-exclusive, paid-up, irrevocable, worldwide license to publish or reproduce the published form of this work, or allow others to do so, for United States Government purposes.

with analytical studies by Huberman and Overhauser [25] and Sergeev [26,27] via different mechanisms of electron scattering at the metal-dielectric interface. Since the pump-probe thermoreflectance measurement technique employed by Stoner and Maris monitored the electronic response to thermal excitations, this explanation seemed viable until molecular dynamics simulations (MDSs) examined the phonon scattering processes affecting h_K . Using classical MDSs, several groups [12,28,29] have found that h_K linearly increases with temperature on a variety of acoustically mismatched interfaces. These classical MDS results, which do not take into account quantum effects (e.g., temperature dependent phonon state filling below the Debye temperature θ_D), conflict with the predictions of the DMM.

The DMM calculations by Stoner and Maris assumed elastic phonon scattering; that is, a phonon of frequency ω in one material will only transfer energy across an interface by scattering with a phonon of frequency ω in the other material. Therefore, the temperature dependence of h_K predictions will be dictated by the phonon population of the lower Debye temperature material. Above the Debye temperature, the phonon population is no longer driven quantum mechanically, but classically [30], which implies a linear dependence on temperature. Therefore, assuming elastic scattering, h_K will be constant at temperatures above the Debye temperature of the lower Debye temperature material at an interface since h_K is proportional to the temperature derivative of the phonon population (this will become more clear in Sec. 2). Since the DMM prediction of constant h_K in the classical limit is a consequence of assuming elastic phonon scattering at the interface, the linear prediction of h_K by the aforementioned MDS studies [28,29] suggests that inelastic phonon scattering events could provide additional means of interfacial transport in the classical limit. Recent experimental studies by Hopkins et al. [7,31] and Lyo and Cahill [8] reported a linear increase in h_K with temperature on a wide range of acoustically mismatched interfaces, supporting the inelastic scattering theory. At heavily mismatched interfaces, h_K was found to exceed the predicted value from the phonon radiation limit (PRL), which estimates the maximum conductance for interfacial transport due to elastic scattering [32]. These experimental studies suggested that the contributions of inelastic scattering mechanisms to h_K could be driven by three (or more) phonon processes at the interface, paralleling the familiar Klemens process between a high energy optical phonon and several lower energy acoustic phonons [33]. However, these experimental studies were performed over a temperature range where either one material or neither material comprising the interface could be considered in the classical limit (or conversely, one or both materials are in the quantum regime); for example, in Lyo and Cahill's experiments on Pb/diamond and Bi/diamond interfaces [8], the reported h_K , however, was only measured from ~ 77 – 300 K, and since the Debye temperatures of Pb, Bi, and diamond are 105 K, 119 K, and 2,230 K, respectively [30], these data represent a regime in which only Pb and Bi are in the classical limit but the diamond substrates were still in the quantum regime. The MDS work, however, only shows evidence of inelastic scattering affecting h_K in the classical limit. Therefore, there are two different regimes where inelastic phonon scattering has been shown to play a role in h_K : the classical regime (MDS work) and the quantum regime (experimental data). As any formulation of h_K based on the DMM, or other models that treat h_K as a derivative of a phonon population, will predict a constant h_K in the classical limit, we focus this work on developing an analytical model to interrogate the role of inelastic scattering in the quantum regime to explain experimentally measured h_K data.

Analytical models for h_K that specifically take into account multiple phonon processes during interfacial transmission in the quantum regime, thereby physically modeling the effects of inelastic scattering on h_K , are lacking [34]. Chen [35] and Dames and Chen [36] developed expressions for phonon transmission that account for inelastic scattering based on the total internal

energy of each phonon system on either side of the interface; these expressions assume that phonons of all energies on both sides of the interface are participating in h_K , which does not consider the specific allowed phonon scattering events governed by energy conservation. Hopkins and Norris [37] developed a joint frequency diffuse mismatch model (JFDMM), which accounts for inelastic scattering by changing the density of states of the phonon flux approaching the interface; again, this model does not specifically examine phonon scattering and conservation during energy transmission. Multiharmonic processes during phonon transmission in a 2D transition layer near the interface were considered by Kosevich [38]; this theory, similar to the JFDMM, assumes that the transition layer allows for vibrational modes around the interface that are not allowed in one of the materials (essentially inelastic scattering), but does not consider phonon scattering or quantum effects in phonon transmission. In another model, Hopkins and Norris [39] separated elastic and inelastic scattering contributions, but their transmission models required experimental h_K data as a function of temperature. Recently, Hopkins [40] developed an analytical model accounting for multiple phonon processes at interfaces; however, this multiple phonon model only considered integer higher harmonics—e.g., for some three-phonon inelastic interfacial process, $\omega_1 + \omega_1 = 2\omega_1$ —and did not consider the more general phonon interfacial process of n phonons of any frequency on one side combining to emit a phonon of frequency $n\omega$ on the other side—e.g., $\omega_1 + \omega_2 = \omega_3$. Although this higher harmonic inelastic model (HHIM) developed by Hopkins explained trends in measured data relatively well, it ignores a potentially substantial avenue for interfacial thermal transport. Obviously, there is a great need for a more general analytical model for h_K that accounts for multiple phonon processes and examines the fundamental phonon physics contributing to inelastic scattering in the quantum temperature regime.

In this paper, a new model for phonon thermal boundary conductance is developed that takes into account inelastic phonon scattering events between two materials by considering energy and phonon number conservation of all phonon frequencies in a thermal flux. This model provides a much more physical representation of the effects of inelastic scattering on h_K than previous models that account for inelastic scattering by considering specific ranges of phonon frequency interactions and by not limiting the interactions to integer harmonic frequencies; thereby, this model considers anharmonic inelastic scattering of phonons at interfaces, and how these processes contribute to thermal boundary conductance. The anharmonic inelastic model (AIM) developed in this work supports the theory that inelastic phonon scattering adds a mechanism for phonon interfacial transport.

The remainder of this paper is separated as follows: Section 2 briefly reviews the DMM and addresses the elastic scattering assumption, and will also derive previous models for inelastic scattering, highlighting the assumptions of phonon interfacial scattering. In Sec. 3, the effect of phonon dispersion on the predictions of these models is addressed, and example calculations are performed for the various elastic and inelastic models reviewed in Sec. 2. In Sec. 4, the AIM is derived and compared with experimental data and previous models. Section 5 concludes this paper by summarizing the major results of the new AIM.

2 Previous Models Accounting for Inelastic Scattering

The various models that account for inelastic scattering discussed in Sec. 1 all assume that the phonons are scattering diffusely at the interface. The new AIM derived in this work also makes this assumption. The diffuse scattering assumption forces scattered modes to lose all memories of polarization and incident angle simplifying the problem to essentially conservation of energy and phonon density considerations. This diffusive scattering assumption is valid due to the thermal wavelength of the phonon system at the temperatures of interest in this work compared with characteristic scattering scales at the interface. The representative

wavelength of the phonon flux approaching the interface can be estimated by the thermal coherence length L , which can be thought of as the spatial extent of the phonon wavepacket [41]. The coherence length for each phonon polarization is given by $L_j \approx \hbar v_j / (k_B T)$, where \hbar is Planck's constant, v is the phonon velocity, k_B is Boltzmann's constant, and j represents the branch or polarization. This coherence length is related to the degree of specularity of the phonon scattering event via [42] $p = \exp[-16\pi^2 \delta_{\text{rms}}^2 / L_j^2]$ where p is the specularity parameter, which estimates the probability that phonons are specularly scattered, and δ_{rms} is the asperity parameter of the interface (mean square deviation of the height of the surface from the reference plane). It is apparent that as the product $\delta_{\text{rms}} T$ increases, the probability of diffuse scattering increases. Also, as the velocity of the phonons in a crystal decreases, the probability of diffuse scattering increases. As previously mentioned, evidence of inelastic scattering has been reported at relatively high temperatures ($T > 50$ K). Diamond, having one of the highest phonon velocities of any pure material (longitudinal velocity of 17,500 m s⁻¹) [43], would therefore be the most likely material to experience specular phonon scattering at an interface. Consider longitudinal diamond phonons approaching an interface at 50 K with only 2 nm of roughness (lattice constant of diamond is approximately 0.357 nm [30], so this is equivalent to only a few monolayers of diamond, which is a conservative, very low estimate for the roughness at diamond surfaces [44]). From the specularity parameter, phonons have less than an 11% probability of scattering specularly at 50 K, with the probability decreasing to 0.01% at 100 K. Therefore, for material systems and temperatures of interest in this work, diffuse phonon scattering is a valid assumption. A more rigorous, generalized discussion on regimes of applicability of the diffusive scattering assumption is discussed by Duda et al. [45].

The remainder of Sec. 2 focuses on derivation of the elastic DMM and compares this model to previously developed models accounting for inelastic scattering, namely, the so-called [46] maximum transmission model (MTM) pioneered by Dames and Chen [36] and the aforementioned HHIM discussed by Hopkins [40]. Although there have been other models derived for inelastic scattering—e.g., the aforementioned JFDMM [37]—and models that represent the upper limits for elastic and inelastic scattering—e.g., the elastic phonon radiation limit [32] and the inelastic phonon radiation limit [39]—we will restrict discussion of the inelastic models in this section to the MTM and HHIM since these two models represent physical upper and lower bounds to inelastic phonon interfacial processes. Several of the elastic and inelastic models not discussed in this section are reviewed in detail by Norris and Hopkins [34].

2.1 The Diffuse Mismatch Model and Elastic Scattering.

The DMM, originally proposed by Swartz and Pohl in 1989 [11], has been derived in detail in several works [11,12,34,45,47], and only highlights of the derivation important for the inelastic models will be focused on here. The phononic flux in isotropic Material 1 approaching the interface between Materials 1 and 2 is given by

$$q_1 = \frac{1}{4} \int_0^{\omega_{c,1}} \hbar \omega \sum_j (v_{1,j}(\omega) D_{1,j}(\omega)) f(\omega) d\omega \quad (1)$$

where \hbar is the reduced Planck's constant, $D(\omega)$ is the volumetric phonon density of states per unit frequency, $f(\omega)$ is the phonon distribution function, $v(\omega)$ is the group velocity of phonons with frequency ω , and $\omega_{c,1}$ is the maximum phonon frequency in Material 1. Taking the transmission probability of the thermal flux across the interface from Side 1 to Side 2 as ζ_1 , the thermal boundary conductance is given by

$$h_K = \frac{1}{4} \int_0^{\omega_{c,1}} \hbar \omega \sum_j (v_{1,j}(\omega) D_{1,j}(\omega)) \frac{\partial f(\omega)}{\partial T} \zeta_1 d\omega \quad (2)$$

since, as per the discussion in Sec. 1, $h_K = q_{\text{int}} / \Delta T$.

The key in evaluating the DMM, or any model discussed in this work, lies in the assumptions invoked when determining ζ_1 . In any model assuming diffuse phonon scattering, the starting point for ζ_1 calculations is the principle of detailed balance [48]. Detailed balance states that for an interface at equilibrium, the net flux must be zero; i.e., $q_{\text{int}}^{1 \rightarrow 2} = q_{\text{int}}^{2 \rightarrow 1}$. An interface that results in purely diffuse scattering can be considered black, and thereby thermalizing, so the interface can be treated as producing a local equilibrium and the phonon population distribution f can be described by a Bose–Einstein distribution [49]. In addition, by the definition of diffuse scattering, $\zeta_2 = 1 - \zeta_1$. An extensive comparison of the various assumptions made when applying the principle of detailed balance to phonon flux across an interface is discussed by Duda et al. [47], but in this work, as with previous works dealing with inelastic scattering, we balance the fluxes of all polarizations approaching the interfaces, thereby upholding the purest assumption of diffusive phonon scattering; i.e., a scattered phonon loses memory of incident polarization. A balance of the total fluxes yields

$$\zeta_1 \int_0^{\omega_{c,1}} \hbar \omega \sum_j (v_{1,j}(\omega) D_{1,j}(\omega)) f(\omega) d\omega = (1 - \zeta_1) \int_0^{\omega_{c,2}} \hbar \omega \sum_j (v_{2,j}(\omega) D_{2,j}(\omega)) f d\omega \quad (3)$$

In the limit of purely elastic scattering, Eq. (3) must be evaluated on a per-frequency basis, since during elastic scattering events, phonons can only emit phonons of equal energies. Therefore, Eq. (3) can be rewritten as

$$\zeta_1 \hbar \omega \sum_j (v_{1,j}(\omega) D_{1,j}(\omega)) f(\omega) = (1 - \zeta_1) \hbar \omega \sum_j (v_{2,j}(\omega) D_{2,j}(\omega)) f(\omega) \quad (4)$$

which is simplified to the well known two-phonon elastic scattering transmission commonly reported as the DMM transmission, given by

$$\zeta_1^{(2)} = \frac{\sum_j (v_{2,j}(\omega) D_{2,j}(\omega))}{\sum_j (v_{1,j}(\omega) D_{1,j}(\omega)) + \sum_j (v_{2,j}(\omega) D_{2,j}(\omega))} \quad (5)$$

Here the superscript (2) denotes that this transmission applies to a two-phonon, elastic process (one phonon on Side 1 couples with one phonon on Side 2). The DMM considering only elastic scattering is therefore given by

$$h_K^{(2)} = \frac{1}{4} \int_0^{\omega_{c,1}} \hbar \omega \sum_j (v_{1,j}(\omega) D_{1,j}(\omega)) \frac{\partial f(\omega)}{\partial T} \zeta_1^{(2)} d\omega \quad (6)$$

2.2 The Maximum Transmission Model. The MTM, proposed by Dames and Chen in 2004 [36], assumes that all phonons of all frequencies in Sides 1 and 2 will participate in thermal transmission. Therefore, detailed balance on the interfacial phonon flux is given in Eq. (3) with no further assumptions. Therefore, the transmission in the MTM is given by

$$\zeta_1^{\text{MTM}} = \frac{\int_0^{\omega_{c,2}} \hbar \omega \sum_j (v_{2,j}(\omega) D_{2,j}(\omega)) f(\omega) d\omega}{\int_0^{\omega_{c,1}} \hbar \omega \sum_j (v_{1,j}(\omega) D_{1,j}(\omega)) f(\omega) d\omega + \int_0^{\omega_{c,2}} \hbar \omega \sum_j (v_{2,j}(\omega) D_{2,j}(\omega)) f(\omega) d\omega} \quad (7)$$

Note that the quantity $\int_0^{\omega_c} \hbar \omega \sum_j (v_j(\omega) D_j(\omega)) f(\omega) d\omega$ is defined as the internal energy of the phonon system [30]. Therefore, in this transmission coefficient derivation of the MTM, energy conservation during individual scattering events is not considered since the entire phonon population in a given side is governed by one transmission probability at a given temperature. This development does not specifically consider the energy conserving processes of several lower frequency phonons in Side 1 scattering at the interface and emitting a high frequency phonon in Side 2, which is the fundamental multiple phonon interfacial process contributing to inelastic scattering during h_K . Therefore, since the MTM transmission is derived considering all possible phonon scattering processes, the thermal boundary conductance predicted by the MTM as follows:

$$h_K^{\text{MTM}} = \frac{1}{4} \int_0^{\omega_{c,1}} \hbar \omega \sum_j (v_{1,j}(\omega) D_{1,j}(\omega)) \frac{\partial f(\omega)}{\partial T} \zeta_1^{\text{MTM}} d\omega \quad (8)$$

can be considered an upper limit to thermal boundary conductance accounting for inelastic processes.

2.3 The Higher Harmonic Inelastic Model. The HHIM, proposed by Hopkins in 2009 [40], takes into account specific multiple phonon processes, or an n phonon process where n is any integer. The HHIM is limited to processes where n phonons of frequency ω scatter simultaneously at an interface and emit a phonon of frequency $n\omega$. An example of a three-phonon process is

then modeled as two phonons of frequency ω emitting a phonon of frequency 2ω . The HHIM represents the first attempt to analytically model specific inelastic processes in the framework of the DMM.

The two-phonon processes in the HHIM are modeled with the DMM (Eq. (6) in Sec. 2.1). In the original derivation of the HHIM, the higher harmonic processes are separated into longitudinal and transverse modes. As this is not consistent with our definition of purely diffuse scattering and the DMM [47], we re-derive the higher harmonic processes in the HHIM in a more consistent formulation.

To begin with our more consistent derivation of the HHIM, we invoke detailed balance on three-phonon higher harmonic processes at the interface between Sides 1 and 2, which gives

$$\begin{aligned} \zeta_1^{(3)} 2\hbar \omega \sum_j (v_{1,j}(\omega) D_{1,j}(\omega)) f(\omega) \\ = (1 - \zeta_1^{(3)}) \hbar (2\omega) \sum_j (v_{2,j}(2\omega) D_{2,j}(2\omega)) f(2\omega) \end{aligned} \quad (9)$$

Equation (9) balances the flux between two phonons of frequency ω from Side 1 and one phonon of frequency 2ω from Side 2. Note that the maximum possible frequency on Side 2 that can contribute to these three-phonon processes is twice that of Side 1. Rearranging Eq. (9) gives the three-phonon transmission coefficient in the HHIM, given by

$$\zeta_1^{(3)} = \frac{\hbar (2\omega) \sum_j (v_{2,j}(2\omega) D_{2,j}(2\omega)) f(2\omega)}{2\hbar \omega \sum_j (v_{1,j}(\omega) D_{1,j}(\omega)) f(\omega) + \hbar (2\omega) \sum_j (v_{2,j}(2\omega) D_{2,j}(2\omega)) f(2\omega)} \quad (10)$$

where, as with the two-phonon transmission probability (Eq. (5)), the three-phonon transmission is frequency dependent. This is unlike the MTM transmission probability, which is dependent only on temperature. Since Eq. (10) represents a transmission probability assuming all phonons are undergoing three-phonon processes, this ignores the effect of elastic scattering. Assuming a perfect interface where phonons only undergo one scattering event, they can lose energy by either scattering with one phonon of the same energy (elastic), or through a three, four, etc., higher order (inelastic) phonon scattering process. Therefore, although Eq. (10) considers the three-phonon process, it does not account for phonons that have already been scattered via elastic processes. The number of phonons at a given frequency that have undergone elastic processes in Sides 1 and 2 is given by

$$N_{1,\text{trans}}^{(2)} = \zeta_1^{(2)} \sum_j (D_{1,j}(\omega)) f(\omega) d\omega \quad (11)$$

and

$$N_{2,\text{trans}}^{(2)} = (1 - \zeta_1^{(2)}) \sum_j (D_{2,j}(\omega)) f(\omega) d\omega \quad (12)$$

respectively. Therefore, the phonons per frequency remaining on Sides 1 and 2 after a two-phonon elastic process is

$$N_{1,\text{remain}}^{(2)} = (1 - \zeta_1^{(2)}) \sum_j (D_{1,j}(\omega)) f(\omega) d\omega \quad (13)$$

and

$$N_{2,\text{remain}}^{(2)} = \zeta_1^{(2)} \sum_j (D_{2,j}(\omega)) f(\omega) d\omega \quad (14)$$

respectively. To determine the phonon transmission due to three-phonon processes, only the phonons remaining must be included in the flux balance. Given that the phonon flux at a frequency ω is related to the number of phonons through $q \propto \hbar \omega v(\omega) N$, detailed balance on the flux participating in three-phonon processes in the framework of the HHIM yields

$$\begin{aligned} & \zeta_1^{(3)} 2\hbar\omega \sum_j (v_{1,j}(\omega)D_{1,j}(\omega))f(\omega)(1 - \zeta_1^{(2)}) \\ & = (1 - \zeta_1^{(3)})\hbar(2\omega) \sum_j (v_{2,j}(2\omega)D_{2,j}(2\omega))f(2\omega)\zeta_1^{(2)} \quad (15) \end{aligned}$$

when $0 < \omega \leq \omega_{c,1}/2$ and

$$\begin{aligned} & \zeta_1^{(3)} 2\hbar\omega \sum_j (v_{1,j}(\omega)D_{1,j}(\omega))f(\omega)(1 - \zeta_1^{(2)}) \\ & = \hbar(2\omega) \sum_j (v_{2,j}(2\omega)D_{2,j}(2\omega))f(2\omega)\zeta_1^{(2)} \quad (16) \end{aligned}$$

when $\omega_{c,1}/2 < \omega \leq \omega_{c,1}$, leading to a three-phonon transmission coefficient defined as

$$\zeta_1^{(3)} = \frac{\hbar(2\omega) \sum_j (v_{2,j}(2\omega)D_{2,j}(2\omega))f(2\omega)\zeta_1^{(2)}}{2\hbar\omega \sum_j (v_{1,j}(\omega)D_{1,j}(\omega))f(\omega)(1 - \zeta_1^{(2)}) + \hbar(2\omega) \sum_j (v_{2,j}(2\omega)D_{2,j}(2\omega))f(2\omega)\zeta_1^{(2)}} \quad (17)$$

when $0 < \omega \leq \omega_{c,1}/2$ and

$$\zeta_1^{(3)} = \frac{\hbar(2\omega) \sum_j (v_{2,j}(2\omega)D_{2,j}(2\omega))f(2\omega)}{2\hbar\omega \sum_j (v_{1,j}(\omega)D_{1,j}(\omega))f(\omega)(1 - \zeta_1^{(2)}) + \hbar(2\omega) \sum_j (v_{2,j}(2\omega)D_{2,j}(2\omega))f(2\omega)} \quad (18)$$

when $\omega_{c,1}/2 < \omega \leq \omega_{c,1}$. Now, the total flux remaining on Side 1 that can participate in three-phonon processes is given by $q_1^{(3)} = \hbar\omega \sum_j (v_{1,j}(\omega)D_{1,j}(\omega))f(\omega)(1 - \zeta_1^{(2)})$. However, when applying detailed balance on the phonon flux, two phonons from Side 1 are balanced with one phonon from Side 2. Therefore, to ensure we are not double counting phonons in the incident flux, the total flux remaining on Side 1 that can participate in higher harmonic phonon processes must be divided by the number of phonons participating in the higher harmonic interfacial scattering event on Side 1, which leads to the remaining flux on Side 1 for three-phonon processes, for example, given by

$$q_1^{(3)} = \frac{1}{2}\hbar\omega \sum_j (v_{1,j}(\omega)D_{1,j}(\omega))f(\omega)(1 - \zeta_1^{(2)}) \quad (19)$$

From Eqs. (17)–(19) the three-phonon thermal boundary conductance in the HHIM is defined as

$$h_K^{(3)} = \frac{1}{8} \int_0^{\omega_{c,1}} \hbar\omega \sum_j (v_{1,j}(\omega)D_{1,j}(\omega)) \frac{\partial f(\omega)}{\partial T} \zeta_1^{(3)} (1 - \zeta_1^{(2)}) d\omega \quad (20)$$

with the number of phonons remaining after the three-phonon inelastic processes on Sides 1 and 2 given by $N_{1,\text{remain}}^{(3)} = (1 - \zeta_1^{(2)}) \times (1 - \zeta_1^{(3)}) \sum_j (D_{1,j}(\omega))f(\omega)d\omega$ and $N_{2,\text{remain}}^{(3)} = \zeta_1^{(2)} \zeta_1^{(3)} \sum_j (D_{1,j}(\omega))f(\omega)d\omega$, respectively.

This thermal boundary conductance is generalized to n harmonic inelastic phonon scattering as

$$h_K^{(n)} = \frac{1}{4(n-1)} \int_0^{\omega_{c,1}} \hbar\omega \sum_j (v_{1,j}(\omega)D_{1,j}(\omega)) \frac{\partial f(\omega)}{\partial T} \zeta_1^{(n)} \times \prod_{s=2}^{n-1} ((1 - \zeta_1^{(s)})) d\omega \quad (21)$$

where the n -phonon transmission coefficient ($n > 2$) is defined as

$$\zeta_1^{(n)} = \begin{cases} \frac{\hbar(n\omega) \sum_j (v_{2,j}(n\omega)D_{2,j}(n\omega))f(n\omega) \prod_{s=2}^{n-1} (\zeta_1^{(s)})}{n\hbar\omega \sum_j (v_{1,j}(\omega)D_{1,j}(\omega))f(\omega) \prod_{s=2}^{n-1} ((1 - \zeta_1^{(s)})) + \hbar(n\omega) \sum_j (v_{2,j}(n\omega)D_{2,j}(n\omega))f(n\omega) \prod_{s=2}^{n-1} (\zeta_1^{(s)})}, & 0 \leq \omega < \frac{\omega_{c,1}}{(n-1)} \\ \frac{\hbar(n\omega) \sum_j (v_{2,j}(n\omega)D_{2,j}(n\omega))f(n\omega) \prod_{s=3}^{n-1} (\zeta_1^{(s)})}{n\hbar\omega \sum_j (v_{1,j}(\omega)D_{1,j}(\omega))f(\omega) \prod_{s=2}^{n-1} ((1 - \zeta_1^{(s)})) + \hbar(n\omega) \sum_j (v_{2,j}(n\omega)D_{2,j}(n\omega))f(n\omega) \prod_{s=3}^{n-1} (\zeta_1^{(s)})}, & \frac{\omega_{c,1}}{(n-1)} \leq \omega < \frac{2\omega_{c,1}}{(n-1)} \\ \vdots \\ \frac{\hbar(n\omega) \sum_j (v_{2,j}(n\omega)D_{2,j}(n\omega))f(n\omega)}{n\hbar\omega \sum_j (v_{1,j}(\omega)D_{1,j}(\omega))f(\omega) \prod_{s=2}^{n-1} ((1 - \zeta_1^{(s)})) + \hbar(n\omega) \sum_j (v_{2,j}(n\omega)D_{2,j}(n\omega))f(n\omega)}, & \frac{(n-2)\omega_{c,1}}{(n-1)} \leq \omega \leq \omega_{c,1} \end{cases} \quad (22)$$

Given Eqs. (21) and (22), the total thermal boundary conductance is calculated by summing all the higher harmonic contributions, mathematically given by

$$h_K = \sum_{m=2}^n h_K^{(m)} \quad (23)$$

Since the HHIM only considers one type of inelastic phonon scattering event at an interface (a higher harmonic scattering process in which n phonons of the same frequency scatter simultaneously), it is the lower bound to inelastic processes. To consider inelastic processes more rigorously, all possible inelastic processes (all types of anharmonic processes including but not limited to higher harmonic scattering) must be considered. This is accounted for in the AIM, which is derived in Sec. 4. In Sec. 3, we show example calculations of the DMM, MTM, and HHIM to lay the framework and show the need for the more rigorous AIM.

3 Example Calculations of Previous Inelastic Models

The starting point of any phononic thermal model is the phonon dispersion, since this gives information about the available phonon frequencies (integration limit), density of states, and group velocity. Assuming f is the Bose–Einstein distribution, the only other piece of information needed to calculate the models in Sec. 2 is the phonon dispersion $\omega(k)$, where k is the phonon wavevector. With the phonon dispersion, the group velocity is given by $v(\omega) = \partial\omega(k)/\partial k$ and the density of states, assuming an isotropic medium, is given by $D(\omega) = k^2/(2\pi^2v(\omega))$. In this work, we assume an isotropic system described by the phononic properties in the (100) direction as it has been shown that the isotropic assumption is valid in the elastic limit [45]. Although a frequently assumed model for phonon frequency as a function of wavevector is the dispersionless Debye model [30], where $\omega(k) = vk$ and v is constant with wavevector and frequency throughout the first Brillouin zone, not accounting for dispersive phonon modes near the zone boundary can lead to an incorrect prediction of phonon thermal flux participating in thermal boundary conductance calculations [18]. A more accurate model, which accounts for these dispersive phonon modes, is the Sine-type model that is derived from the equations of motion of a one-dimensional chain of masses-on-springs [30]. This model has been shown to successfully predict the heat capacity and mean free path of bulk materials [50,51], and therefore, represents a good approximation of phononic dispersion to obtain closed-form solutions for our thermal boundary conductance models. The Sine-type dispersion for fcc or diamond cubic crystal structures in the (100) direction is given by

$$\omega(k) = \omega_c \sin\left[\frac{ka}{4}\right] \quad (24)$$

where a is the lattice spacing, and the corresponding phonon group velocity is given by

$$v(k) = \frac{\omega_c a}{4} \cos\left[\frac{ka}{4}\right] \quad (25)$$

Since we have formulated the models in Sec. 2 in frequency space, we convert Eq. (25) to the frequency domain by rearranging Eq. (24) to yield $k = (4/a)\sin^{-1}[\omega/\omega_c]$ giving the phononic group velocity as

$$v(\omega) = \frac{\omega_c a}{4} \sqrt{1 - \left(\frac{\omega}{\omega_c}\right)^2} \quad (26)$$

and the density of states as

$$D(\omega) = \frac{2k^2}{\pi\omega_c a \sqrt{1 - \left(\frac{\omega}{\omega_c}\right)^2}} \quad (27)$$

With Eqs. (26) and (27), we can solve all the models presented in this work given the lattice spacing and maximum frequencies in the materials of interest.

The example calculations that we perform in this work will focus on the Pb/diamond interface, since h_K across the interface of these largely acoustically mismatched materials has not only been measured experimentally [8], but the experimental results suggest that inelastic phonon scattering processes are playing a significant role in interfacial energy transport [39]. In addition, the basic formulation of the DMM and the diffuse transmission coefficient is valid in acoustically mismatched materials and describes the two-phonon elastic transmission process at the Pb/diamond interface extremely well [39]. The average lattice constants in Pb and diamond are taken as 0.495 nm and 0.357 nm, respectively [30]. We take the maximum phonon frequencies (ω_c) in Pb from measured data [52] and those in diamond from lattice dynamics [53]. As previously mentioned, for model calculations, we assume an isotropic medium and determine the maximum phonon frequencies in the (100) direction from the dispersion data (note, in crystal structures with cubic symmetries, the transverse branches are degenerate in the (100) direction). The maximum longitudinal and transverse frequencies are 13.6 Trad s^{-1} and 7.1 Trad s^{-1} , respectively, for Pb and 224 Trad s^{-1} and 148 Trad s^{-1} , respectively, for diamond. We need not consider the optical phonons in diamond for these calculations since these energies contribute minimally to the phonon flux in the temperature range of interest in this study (50–550 K corresponding to the measured data on Pb/diamond [8]). To verify this assumption regarding the lack of participation of the optical phonon's in h_K for the temperature range of interest, we calculate the following quantity at 550 K: $1 - (\int_0^{\omega_{2,c}} f d\omega) / (\int_0^{\omega_c} f d\omega) \approx 0.002$, where f is the Bose–Einstein distribution function and $\omega_{2,c} = 224$ Trad s^{-1} is the maximum acoustic phonon frequency in diamond. As this quantifies the fraction of modes above the maximum acoustic phonon frequency in diamond that can participate at 550 K, we determine that the maximum contribution of optical modes is less than 0.2 % at 550 K, with decreasing participation at lower temperatures.

To evaluate the accuracy of the assumed phonon dispersion on model calculations, we calculate the phonon thermal flux incident on the Pb/diamond interface with the Debye and Sine-type dispersion models. Effectively, this is the thermal flux for Pb calculated with Eq. (1). Given that both the Debye and Sine-type models are approximations to the phonon dispersion, to evaluate our assumptions, we compare these calculations to flux calculations using an exact dispersion relation by fitting the measured dispersion in Pb in the (100) direction with fourth degree polynomials. These polynomials are given by $\omega(k) = 6.056 \times 10^{-28}k^4 - 1.926 \times 10^{-17}k^3 + 4.782 \times 10^{-8}k^2 + 2.187 \times 10^3k$ for the longitudinal branch and $\omega(k) = 6.827 \times 10^{-28}k^4 - 1.912 \times 10^{-17}k^3 + 7.927 \times 10^{-8}k^2 + 1.114 \times 10^3k$ for the transverse branch. For Debye calculations, we take the zone center group velocity from the measured dispersion (i.e., 2187 m s^{-1} and 1114 m s^{-1} for the longitudinal and transverse modes, respectively) and calculate the maximum phonon frequency for each phonon branch as $\omega_{c,j} = v_j(6\pi^2n)^{1/3}$, where v is the constant group velocity used in the Debye calculations and n is the lattice point density, to be consistent with Debye theory [30].

Figure 1 shows the predicted thermal flux in Pb using the Sine-type and Debye dispersion models normalized by the predicted thermal flux using the polynomial dispersion relation (q_{real}). The Sine-type dispersion gives a much more realistic prediction of the thermal flux than the Debye dispersion. The Debye dispersion overpredicts the thermal flux by a factor of 1.5–2 in the temperature range of interest. Given that experimental trends of h_K at Pb/diamond interfaces suggest that inelastic phonon scattering

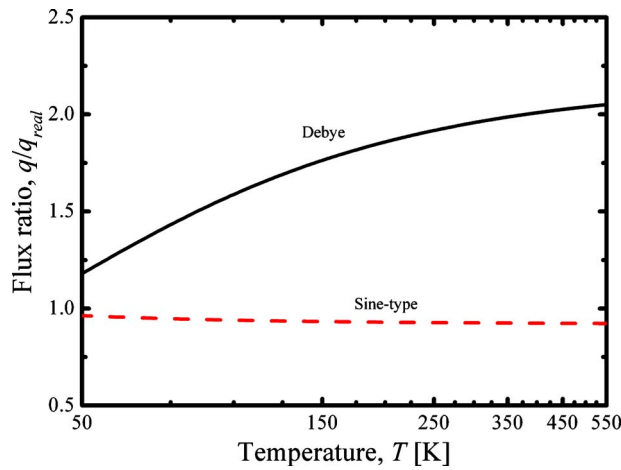


Fig. 1 Predicted thermal flux in Pb using the Sine-type and Debye dispersion models normalized by the predicted thermal flux using the polynomial dispersion relation from phonon dispersion data (q_{real}). The Sine-type dispersion gives a much more realistic prediction of the thermal flux than the Debye dispersion. The use of the Debye dispersion model in these calculations would result in a nonphysical overprediction of the actual thermal flux in Pb, and therefore an overprediction of h_K at the Pb/diamond interface.

leads to the large value (compared with the elastic DMM) and the linear temperature trend, use of a Debye dispersion in these calculations would result in a nonphysical better-agreement between the data and the models. Note that we choose to use the Sine-type dispersion as opposed to a realistic dispersion in our model calculations to focus on the conceptual model development and to present analytically tractable models; the use of a polynomial dispersion derived from measured dispersion data in thermal boundary conductance calculations requires additional considerations of phonon coupling [45], even in the elastic limit, and would distract from the inelastic phonon model development discussed in this work.

With the Sine-type dispersion, the DMM, MTM, and HHIM are calculated for the Pb/diamond interface. These calculations are shown in Fig. 2 along with experimental data of measured h_K at the Pb/diamond interface and h_K at the interface between Pb and hydrogen-terminated diamond (Pb/H/diamond) [8]. The DMM not only underpredicts the experimental data (by nearly an order of magnitude at room temperature), but also fails to capture the increasing trend in h_K with temperature. Since the DMM only accounts for two-phonon elastic scattering, it does not account for the additional avenues of conductance from the inelastic processes. In addition, assuming elastic scattering, no phonons above the maximum phonon frequency in Pb can participate in h_K , and therefore the DMM predictions saturate with the heat capacity in Pb, that is, around the Debye temperature (~ 105 K) [30].

The HHIM takes into account inelastic phonon processes, and therefore predicts a higher value of h_K since these additional phonon processes are able to transmit heat across the Pb/diamond interface. In addition, by considering the contributions of the inelastic phonon processes, the HHIM predicts a temperature dependence above the Debye temperature of Pb while DMM predictions are constant with temperature above the Debye temperature of Pb. The temperature dependency derives from the fact that phonons in diamond with frequencies higher than the maximum frequency in Pb are able to participate in the higher harmonic inelastic processes modeled in the HHIM. Contributions of processes involving up to five phonons are considered in HHIM calculations of h_K (expressed in Eq. (23) with $n=5$). Each higher harmonic contribution to the total h_K is shown in the inset of Fig. 2.

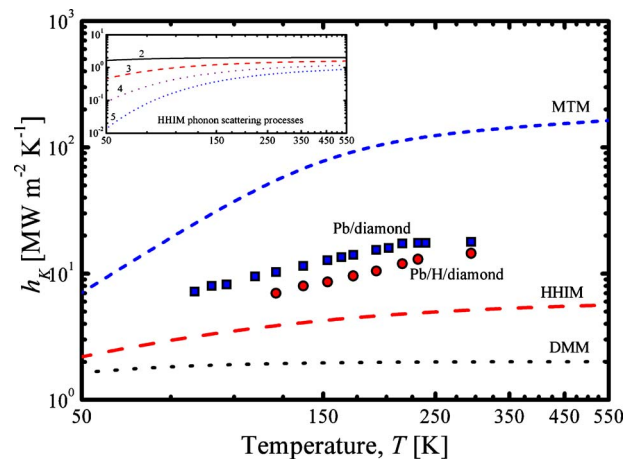


Fig. 2 DMM, MTM, and HHIM calculations for h_K at a Pb/diamond interface using the Sine-type dispersion along with experimental data of measured h_K at the Pb/diamond interface and h_K at the interface between Pb and hydrogen-terminated diamond (Pb/H/diamond) [8]. The DMM not only underpredicts the experimental data but also does not capture the increasing trend in h_K with temperature since it only accounts for two-phonon elastic scattering. The MTM greatly overpredicts the experimental data since all phonons of all frequencies in diamond are assumed to participate in h_K , where the underprediction of the HHIM is due to only accounting for one type of inelastic scattering event (i.e., the higher harmonic process). Inset: each higher harmonic contribution to the total h_K predicted by the HHIM.

The MTM greatly overpredicts the experimental data. It predicts much higher values than the experimentally measured h_K (nearly an order of magnitude higher at room temperature), and, although it predicts a temperature dependent trend above the Debye temperature of Pb, the trend is nonlinear and steeper compared with the linear temperature dependent trends in the measured data. The overpredictions in values and differing temperature trends of the MTM arise because all phonons of all frequencies in diamond are assumed to participate in h_K , where the corresponding properties' underpredictions in the HHIM are due to only accounting for one type of inelastic scattering event (i.e., the higher harmonic process). Clearly, a more rigorous model that accounts for all types of inelastic scattering events while also tracking phonon population change to determine the phonon frequencies that can participate in specific inelastic scattering processes would remedy the shortcomings of both the MTM and HHIM. These aspects of interfacial phonon scattering and their contributions to h_K are key components to the anharmonic inelastic model, derived in Sec. 4.

4 The Anharmonic Inelastic Model

The AIM is derived in a similar framework as the HHIM, such that phonon number conservation is considered, but since all inelastic phonon scattering events are considered, the transmission probabilities are calculated through a slightly different flux balance. In the AIM, the two-phonon elastic scattering contribution to h_K is still calculated with the DMM (Eqs. (5) and (6)), and therefore the number of phonons at a given frequency that have undergone elastic processes from Sides 1 and 2 is still described in Eqs. (11) and (12), respectively, and those remaining on Sides 1 and 2 are described in Eqs. (13) and (14), respectively. However, to determine the phonon transmission due to three-phonon processes, all possible remaining phonon frequencies that can participate in three-phonon inelastic interfacial processes must be considered. Therefore, detailed balance on all phonons in the remaining flux participating in three-phonon processes yields

$$\begin{aligned} \zeta_1^{(3)} \int_0^{\omega_{c,1}} 2\hbar\omega \sum_j (v_{1,j}(\omega)D_{1,j}(\omega))f(\omega)(1 - \zeta_1^{(2)})d\omega &= (1 - \zeta_1^{(3)}) \\ &\times \left(\int_0^{\omega_{c,1}} \hbar\omega \sum_j (v_{2,j}(\omega)D_{2,j}(\omega))f(\omega)\zeta_1^{(2)}d\omega \right. \\ &\left. + \int_{\omega_{c,1}}^{2\omega_{c,1}} \hbar\omega \sum_j (v_{2,j}(\omega)D_{2,j}(\omega))f(\omega)d\omega \right) \end{aligned} \quad (28)$$

where the total flux on Side 2 is only integrated up to twice the maximum phonon frequency in Side 1, since $2\omega_{c,1}$ represents the maximum possible phonon frequency resulting from scattering of any two phonons in Side 1. Rearranging Eq. (28) leads to the AIM three-phonon transmission coefficient, given by

$$\begin{aligned} \zeta_1^{(3)} &= \left(\int_0^{\omega_{c,1}} \hbar\omega \sum_j (v_{2,j}(\omega)D_{2,j}(\omega))f(\omega)\zeta_1^{(2)}d\omega \right. \\ &+ \int_{\omega_{c,1}}^{2\omega_{c,1}} \hbar\omega \sum_j (v_{2,j}(\omega)D_{2,j}(\omega))f(\omega)d\omega \left. \right) \\ &\times \left(\int_0^{\omega_{c,1}} 2\hbar\omega \sum_j (v_{1,j}(\omega)D_{1,j}(\omega))f(\omega)(1 - \zeta_1^{(2)}) \right. \\ &+ \left(\int_0^{\omega_{c,1}} \hbar\omega \sum_j (v_{2,j}(\omega)D_{2,j}(\omega))f(\omega)\zeta_1^{(2)}d\omega \right. \\ &\left. \left. + \int_{\omega_{c,1}}^{2\omega_{c,1}} \hbar\omega \sum_j (v_{2,j}(\omega)D_{2,j}(\omega))f(\omega)d\omega \right) \right)^{-1} \end{aligned} \quad (29)$$

As with our discussion in Sec. 2, the total flux remaining that will participate in three-phonon inelastic scattering described in Eq. (29) is given by

$$q_1^{(3)} = \frac{1}{2}\hbar\omega \sum_j (v_{1,j}(\omega)D_{1,j}(\omega))f(\omega)(1 - \zeta_1^{(2)}) \quad (30)$$

leading to a three-phonon thermal boundary conductance in the AIM defined as

$$h_K^{(3)} = \frac{1}{8} \int_0^{\omega_{c,1}} \hbar\omega \sum_j (v_{1,j}(\omega)D_{1,j}(\omega)) \frac{\partial f(\omega)}{\partial T} \zeta_1^{(3)} (1 - \zeta_1^{(2)}) d\omega \quad (31)$$

Similarly, for four-phonon inelastic processes, the transmission coefficient is given by

$$\begin{aligned} \zeta_1^{(4)} &= \left(\int_0^{\omega_{c,1}} \hbar\omega \sum_j (v_{2,j}(\omega)D_{2,j}(\omega))f(\omega)\zeta_1^{(2)}\zeta_1^{(3)}d\omega \right. \\ &+ \int_{\omega_{c,1}}^{2\omega_{c,1}} \hbar\omega \sum_j (v_{2,j}(\omega)D_{2,j}(\omega))f(\omega)\zeta_1^{(3)}d\omega \\ &+ \int_{2\omega_{c,1}}^{3\omega_{c,1}} \hbar\omega \sum_j (v_{2,j}(\omega)D_{2,j}(\omega))f(\omega)d\omega \left. \right) \\ &\times \left(\int_0^{\omega_{c,1}} 3\hbar\omega \sum_j (v_{1,j}(\omega)D_{1,j}(\omega))f(\omega)(1 - \zeta_1^{(2)})(1 - \zeta_1^{(3)}) \right. \\ &+ \int_0^{\omega_{c,1}} \hbar\omega \sum_j (v_{2,j}(\omega)D_{2,j}(\omega))f(\omega)\zeta_1^{(2)}\zeta_1^{(3)}d\omega \\ &\left. + \int_{\omega_{c,1}}^{2\omega_{c,1}} \hbar\omega \sum_j (v_{2,j}(\omega)D_{2,j}(\omega))f(\omega)\zeta_1^{(3)}d\omega \right) \end{aligned}$$

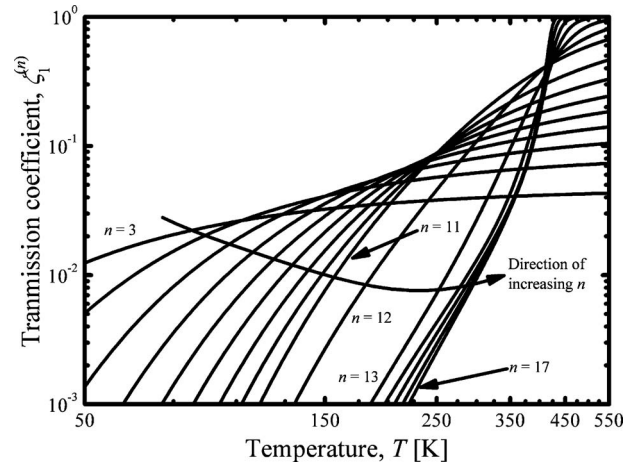


Fig. 3 AIM n -phonon transmission coefficient calculations for various values of n for the Pb/diamond interface as a function of temperature calculated with Eq. (35). In general, the transmission probability of higher order processes increases with increasing temperature. As temperature is increased, the number of modes in diamond at any frequency increases, and therefore the transmission coefficient increases. Eventually, for the higher n processes at high temperatures, all of the Pb phonons become exhausted and the transmission coefficient become unity.

$$+ \int_{2\omega_{c,1}}^{3\omega_{c,1}} \hbar\omega \sum_j (v_{2,j}(\omega)D_{2,j}(\omega))f(\omega)d\omega \left. \right)^{-1} \quad (32)$$

leading to a four-phonon thermal boundary conductance given by

$$\begin{aligned} h_K^{(4)} &= \frac{1}{12} \int_0^{\omega_{c,1}} \hbar\omega \sum_j (v_{1,j}(\omega)D_{1,j}(\omega)) \frac{\partial f(\omega)}{\partial T} \\ &\times \zeta_1^{(4)} (1 - \zeta_1^{(2)}) (1 - \zeta_1^{(3)}) d\omega \end{aligned} \quad (33)$$

This thermal boundary conductance is generalized to any n -phonon inelastic scattering process as

$$\begin{aligned} h_K^{(n)} &= \frac{1}{4(n-1)} \int_0^{\omega_{c,1}} \hbar\omega \sum_j (v_{1,j}(\omega)D_{1,j}(\omega)) \frac{\partial f(\omega)}{\partial T} \zeta_1^{(n)} \\ &\times \prod_{s=2}^{n-1} ((1 - \zeta_1^{(s)})) d\omega \end{aligned} \quad (34)$$

similar to the HHIM, but the n -phonon transmission coefficient ($n > 2$) is defined as

$$\begin{aligned} \zeta_1^{(n)} &= \sum_{i=0}^{n-1} \int_i^{(i+1)\omega_{c,1}} \hbar\omega \sum_j (v_{2,j}(\omega)D_{2,j}(\omega))f(\omega) \prod_{s=i+2}^{n-1} (\zeta_1^{(s)})d\omega \\ &\times \left((n-1) \int_0^{\omega_{c,1}} \hbar\omega \sum_j (v_{1,j}(\omega)D_{1,j}(\omega))f(\omega) \prod_{s=2}^{n-1} ((1 - \zeta_1^{(s)}))d\omega \right. \\ &\left. + \sum_{i=0}^{n-1} \int_i^{(i+1)\omega_{c,1}} \hbar\omega \sum_j (v_{2,j}(\omega)D_{2,j}(\omega))f(\omega) \prod_{s=i+2}^{n-1} (\zeta_1^{(s)})d\omega \right)^{-1} \end{aligned} \quad (35)$$

Figure 3 shows calculations of Eq. (35) for various values of n for the Pb/diamond interface as a function of temperature. We estimate the maximum n by dividing the cutoff frequency of the longitudinal acoustic branch in diamond by the cutoff frequency of the longitudinal acoustic branch in Pb (224 Trad s^{-1})

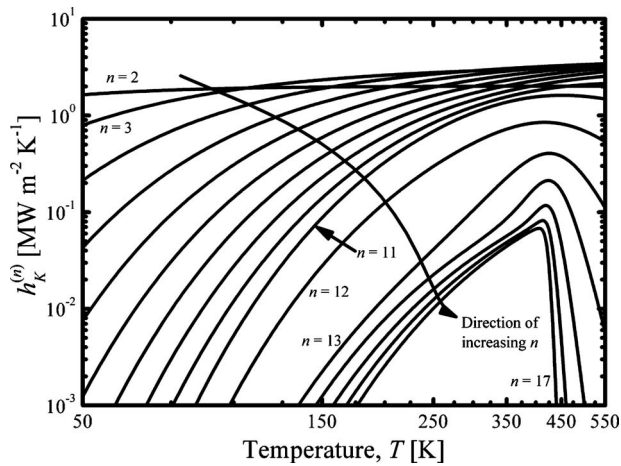


Fig. 4 AIM predictions of $h_K^{(n)}$ as a function of temperature (Eq. (34)) for Pb/diamond for $n=2-17$. Note that the change in temperature trends of the n -phonon transmission coefficient propagate through the $h_K^{(n)}$ calculations as seen in the changing temperature trends beginning with the $n=12$ calculations. Also, note that the contributions from the $n=12$ and higher processes are over an order of magnitude smaller than the contributions from the $n<12$ processes, especially at higher temperatures. This is due to the fact that, in addition to much of the Pb phonon population being exhausted, energetic selection rules allow only high frequency, low group velocity modes in Pb to participate in these higher n processes, which decreases the incident flux and subsequent thermal boundary conductance.

$/13.6 \text{ Trad s}^{-1} \approx 16-17$), so we show the n -phonon transmission coefficient $\zeta_1^{(n)}$ calculations over the range $n=3-17$. Note that we do not use Eq. (35) for $n=2$ since we know the form of the two-phonon elastic transmission coefficient (Eq. (5)) and therefore it is dependent on frequency alone and not temperature. The higher order transmission probabilities defined in Eq. (35) are not dependent on frequency but are dependent on temperature. In general, the transmission probability of higher order processes increases with increasing temperature. The change in trends starting at the $n=12$ transmission probabilities arise due to the exhaustion of the available transverse modes in diamond. As temperature increases, the number of modes in diamond available for interfacial coupling increases. At relatively low temperatures, the number of phonons in Pb far outweighs the number of phonons in diamond. Therefore, phonon frequencies in diamond can become exhausted from “being used up” by lower energy phonons in Pb undergoing anharmonic coupling. As there is a large peak in the density of states of diamond corresponding to transverse modes, once these available transverse phonons have undergone inelastic scattering processes with phonons in Pb, there will be a change in the trend of the transmission coefficient. This is further verified by considering the phonon frequencies in Pb and diamond, i.e., the maximum frequency of the transverse mode in diamond divided by the maximum frequency of the longitudinal mode in Pb: $148 \text{ Trad s}^{-1}/13.6 \text{ Trad s}^{-1} \approx 11$. Therefore, a 12 phonon process (that is $11+1$ since 11 phonons in Pb will couple with 1 phonon in diamond) will mark the onset of different temperature dynamics and trends in $\zeta_1^{(n)}$. As temperature increases, the number of modes in diamond at any frequency increases, and therefore the transmission coefficient increases. Eventually, for the higher n processes at high temperatures, all of the Pb phonons become exhausted and the transmission coefficient goes to unity.

Although the transmission coefficient goes to unity at high temperatures for the higher n processes, this does not necessarily mean that the thermal boundary conductance associated with these processes is substantial, as seen in Fig. 4. Figure 4 shows the

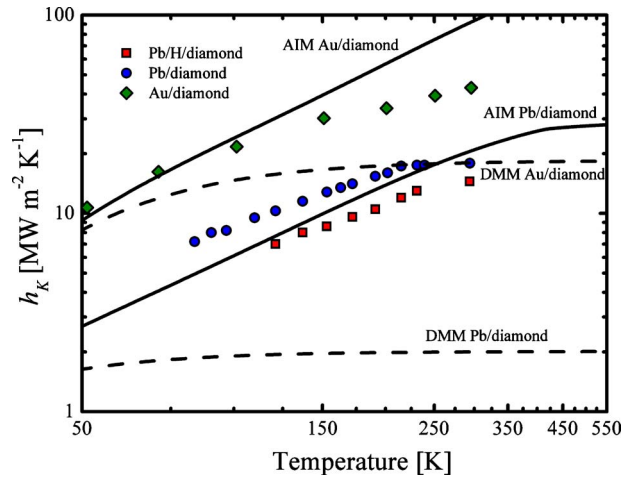


Fig. 5 Total thermal boundary conductance for Pb/diamond and Au/diamond predicted from the AIM calculations using Eq. (23) compared with DMM predictions along with the Pb/diamond [8] and Au/diamond [24] experimental data. The AIM shows improved agreement compared with the DMM with the experimental data, and represents a significant improvement in modeling inelastic contributions to h_K compared with the MTM and HHIM (cf. Fig. 2 for Pb/diamond comparisons).

predictions of $h_K^{(n)}$ as a function of temperature (Eq. (34)) for values of n ranging from 2 to 17. Note that the change in temperature trends of $\zeta_1^{(n)}$ propagates through the $h_K^{(n)}$ calculations as seen in the changing temperature trends beginning with the $n=12$ calculations. Also, note that the contributions from the $n=12$ and higher processes are over an order of magnitude smaller than the contributions from the $n<12$ processes, especially at higher temperatures. This is due to the fact that, in addition to much of the Pb phonon population being exhausted, energetic selection rules allow only high frequency modes in Pb to participate in these higher n processes; even though the transmission coefficient is unity in this regime, the flux is nearly zero since, due to crystal dispersion, the high frequency modes have a significantly reduced group velocity and therefore these processes make negligible contributions to h_K . Compared with the HHIM, the AIM predicts much larger contributions to interfacial thermal transport for the $n=3, 4, 5$ phonon processes. This is intuitive since the AIM accounts for all types of inelastic scattering processes, both higher harmonic and anharmonic (e.g., two phonons of any frequency on Side 1— ω_1 and ω_2 —will emit a phonon of frequency $\omega_1 + \omega_2$ into Side 2), whereas the HHIM only accounts for higher harmonic inelastic scattering (e.g., two phonons of frequency ω_1 on Side 1 will emit a phonon of frequency $2\omega_1$ into Side 2). Because of this, the higher order inelastic processes are predicted to significantly contribute to the overall h_K .

The total thermal boundary conductance predicted from the AIM calculations in Fig. 4 is determined from Eq. (23). These AIM calculations, shown in Fig. 5, are compared with the DMM along with the experimental data. The AIM shows excellent agreement with the experimental data, and represents a significant improvement in modeling inelastic contributions to h_K compared with the MTM and HHIM (cf. Fig. 2). Note that there are no fitting or scaling parameters associated with the AIM, as the only inputs to this model are the phonon dispersion and lattice spacing, which can easily be found in literature. At the Pb/diamond interface, the AIM predicts that inelastic scattering processes involving up to ten phonons will contribute to the overall h_K , explaining not only the reported values but also the temperature trends. As the temperature increases, the number of high energy phonons in diamond increases and the temperature trends in h_K follow the increase in population of these higher energy diamond phonon

modes. To further validate our calculations, we calculate the AIM for the Au/diamond interface and compare these calculations to the experimental data by Stoner and Maris [24] and DMM calculations. As with the Pb/diamond calculations, the Au/diamond AIM calculations agree very well with the measured experimental data and capture the inelastic trends, much improved over DMM predictions. The deviation between the AIM predictions and the measured Au/diamond data at higher temperatures could be due to subsurface damage in the particular diamond substrate used in the measurements by Stoner and Maris, as discussed in their manuscript [24]. For Au, we assume longitudinal and transverse cutoff frequencies of 28.9 Trad s^{-1} and 17.2 Trad s^{-1} and a lattice spacing of 0.408 nm . Although the Bi/diamond thermal boundary conductance measured by Lyeo and Cahill [8] also exhibited inelastic trends, due to the complex unit cell of bismuth (rhombohedral structure), predictions of this interface's h_K are not pursued here since the implementation of the algorithm presented in this work assumed a cubic structure for both materials. However, we emphasize that the algorithm prescribed in this work for the AIM is in a general formulation and can be applied to any type of material system given the proper Brillouin zone and dispersion representation. For example, a full Brillouin zone representation of a crystal's dispersion via lattice dynamics could be used to calculate the inelastic phonon contributions to thermal boundary conductance via the AIM presented in this work, similar to the elastic calculations performed by Reddy et al. [18] using an exact phonon dispersion.

We reemphasize that this model explains the contributions to thermal boundary conductance from inelastic scattering in the quantum regime; in the Pb/diamond example, the temperatures we are interested in ($50\text{--}550 \text{ K}$) are lower than the Debye temperature of diamond indicating that the phonon states in diamond are populating quantum mechanically. This is what drives the temperature trend of h_K in this regime. Molecular dynamics simulations cannot predict thermal boundary conductance in this regime since MDs are a classical technique and attempts at quantum corrections in MDs fail to properly account for phonon mode population changes [54]. Given this, there is currently a disconnect between the regimes that the AIM and MDS can predict, indicating that, as a first step of bridging analytical models for h_K with MDS predictions, interfacial phonon scattering must be further studied in the classical limit.

This inelastic model presented in his work is an extension of the DMM, which assumes that all phonons will scatter at the interface. In reality, scattering processes on either side of the interface could, in fact, affect the flux approaching the interface [12]. However, as no closed-form model for thermal boundary conductance exists that properly accounts for this phenomena, a model that accounts for this type of anharmonic scattering event and its affect on thermal boundary conductance is beyond the scope of this paper. We reemphasize that the AIM derived in this work takes the basic DMM formulation considering an unmodified flux of phonons approaching an interface in which all phonons must scatter.

Following this scattering discussion, we note that the aspect of the DMM in which all phonons must scatter dictates the scattering probability of the incident flux. Since the DMM formulation imposes scattering on all phonons in the incident flux, the selection rules of the different scattering processes across the interface are driven by the available energy states. In this context, we have introduced new interfacial selection rules for anharmonic scattering processes at an interface in which all phonons must scatter. Note that these rules are intrinsically different than the selection rules in a bulk solid. For example, three-phonon processes are the dominant resistive lattice-processes in bulk solid, with the probability of four-phonon processes decreasing rapidly, even at high temperatures. However, in these processes (assuming a perfect crystal with no impurities), there is no spatially restrictive scattering mechanism and the three- and higher order phonon scattering

processes are purely dictated by the crystal potential. Based on restrictions of atomic vibrations, any processes higher than four-phonon processes are very unlikely to occur, even at high temperatures in a bulk solid (in fact, four-phonon processes are very unlikely, and often not considered, in many thermal transport analyses of bulk solids). However, at an interface between two materials, there is a change in the crystal potential, which naturally will induce scattering events. Assuming that all these scattering events occur at the interface, which is the underlying assumption of the DMM, then traditional phonon selection rules in the bulk of a solid break down, and the interfacial scattering selection rules will be based on energy state density, as previously mentioned. These selection rules are the basis of the discussion of the AIM. Note that the HHIM also imposes similar selection rules for high order phonon processes, although the HHIM is more restrictive in their selection rules since the HHIM only allows phonons of equal frequency to participate in scattering events, where the formation of the AIM allows several phonons of different frequencies to scatter at an interface and emit a single phonon on the other side.

5 Conclusions

A new model for phonon thermal boundary conductance h_K is developed that takes into account inelastic phonon scattering events between two materials. Previous models for h_K only consider elastic phonon scattering events (DMM) or do not account properly for all possible phonon scattering events (MTM and HHIM). This new model, the AIM, provides a much more physical consideration of the effects of inelastic scattering on h_K than the previous models by considering specific ranges of phonon frequency interactions and not limiting these interactions to integer harmonic frequencies; thereby, this model considers anharmonic inelastic scattering of phonons at interfaces and their contributions to interfacial transport. The AIM shows improved agreement over the DMM when the model predictions and experimental data are compared for the Pb/diamond and Au/diamond interfaces due to AIM's ability to account for the temperature dependency of the phonon population in diamond, which can couple anharmonically with multiple phonons in Pb and Au. At the Pb/diamond interface, the AIM predicts that inelastic scattering processes involving up to ten phonons will contribute to the overall h_K .

Acknowledgment

P.E.H. is appreciative for funding from the LDRD program office through the Sandia National Laboratories Harry S. Truman Fellowship. J.C.D. gratefully acknowledges financial support from the National Science Foundation through the Graduate Research Fellowship Program. J.C.D. and P.M.N. acknowledge the financial support of Air Force Office of Scientific Research (Grant No. FA9550-09-1-0245). This manuscript has been authored by Sandia Corporation under Contract No. DE-AC04-94AL85000 with the U.S. Department of Energy. Sandia is a multiprogram laboratory operated by Sandia Corporation, a wholly owned subsidiary of Lockheed-Martin Corporation, for the United States Department of Energy's National Nuclear Security Administration under Contract No. DE-AC04-94AL85000.

Nomenclature

- a = lattice spacing, m
- D = volumetric density of states per unit frequency, $\text{m}^{-3} \text{ s}^{-1}$
- f = phonon distribution function
- h = Planck's constant, J s
- \hbar = reduced Planck's constant, J s
- h_K = thermal boundary conductance or Kapitza conductance, $\text{W m}^{-2} \text{ K}^{-1}$
- k = phonon wavevector, m^{-1}
- k_B = Boltzmann's constant, J K^{-1}

L = phonon coherence length, m
 N = phonon number density, m^{-3}
 p = specularity parameter
 q = thermal flux, $W\ m^{-2}$
 R_K = thermal boundary resistance or Kapitza resistance, $W^{-1}\ m^2\ K$
 T = temperature, K
 v = phonon group velocity, $m\ s^{-1}$

Greek Symbols

Δ = change in
 δ_{rms} = asperity parameter, m
 ω = phonon angular frequency, $rad\ s^{-1}$

Subscripts

1 = of Side 1
2 = of Side 2
 C = cutoff frequency
int = interfacial
trans = transmitted
real = realistic
remain = remaining

Superscript

(n) = n -phonon process

References

- Cahill, D. G., Ford, W. K., Goodson, K. E., Mahan, G. D., Majumdar, A., Maris, H. J., Merlin, R., and Phillpot, S. R., 2003, "Nanoscale Thermal Transport," *J. Appl. Phys.*, **93**, pp. 793–818.
- Chang, C. W., Okawa, D., Garcia, H., Majumdar, A., and Zettl, A., 2008, "Breakdown of Fourier's Law in Nanotube Thermal Conductors," *Phys. Rev. Lett.*, **101**, p. 075903.
- Prasher, R. S., 2008, "Thermal Boundary Resistance and Thermal Conductivity of Multiwalled Carbon Nanotubes," *Phys. Rev. B*, **77**, p. 075424.
- Lee, S.-M., Cahill, D. G., and Venkatasubramanian, R., 1997, "Thermal Conductivity of Si-Ge Superlattices," *Appl. Phys. Lett.*, **70**, pp. 2957–2959.
- Li, D., Wu, Y., Fan, R., Yang, P., and Majumdar, A., 2003, "Thermal Conductivity of Si/SiGe Superlattice Nanowires," *Appl. Phys. Lett.*, **83**, pp. 3186–3188.
- Gundrum, B. C., Cahill, D. G., and Averback, R. S., 2005, "Thermal Conductance of Metal-Metal Interfaces," *Phys. Rev. B*, **72**, p. 245426.
- Hopkins, P. E., Stevens, R. J., and Norris, P. M., 2008, "Influence of Inelastic Scattering at Metal-Dielectric Interfaces," *ASME J. Heat Transfer*, **130**, p. 022401.
- Lyeo, H.-K., and Cahill, D. G., 2006, "Thermal Conductance of Interfaces Between Highly Dissimilar Materials," *Phys. Rev. B*, **73**, p. 144301.
- Kapitza, P. L., 1941, "The Study of Heat Transfer in Helium II," *Zh. Eksp. Teor. Fiz. Pis'ma Red.*, **11**, pp. 1–31.
- Little, W. A., 1959, "The Transport of Heat Between Dissimilar Solids at Low Temperatures," *Can. J. Phys.*, **37**, pp. 334–349.
- Swartz, E. T., and Pohl, R. O., 1989, "Thermal Boundary Resistance," *Rev. Mod. Phys.*, **61**, pp. 605–668.
- Landry, E., and Mcgaughey, A. J. H., 2009, "Thermal Boundary Resistance Predictions From Molecular Dynamics Simulations and Theoretical Calculations," *Phys. Rev. B*, **80**, p. 165304.
- Swartz, E. T., and Pohl, R. O., 1987, "Thermal Resistances at Interfaces," *Appl. Phys. Lett.*, **51**, pp. 2200–2202.
- Costescu, R. M., Wall, M. A., and Cahill, D. G., 2003, "Thermal Conductance of Epitaxial Interfaces," *Phys. Rev. B*, **67**, p. 054302.
- Koh, Y. K., and Cahill, D. G., 2007, "Frequency Dependence of the Thermal Conductivity of Semiconductor Alloys," *Phys. Rev. B*, **76**, p. 075207.
- Hopkins, P. E., Norris, P. M., Stevens, R. J., Beechem, T., and Graham, S., 2008, "Influence of Interfacial Mixing on Thermal Boundary Conductance Across a Chromium/Silicon Interface," *ASME J. Heat Transfer*, **130**, p. 062402.
- Stevens, R. J., Smith, A. N., and Norris, P. M., 2005, "Measurement of Thermal Boundary Conductance of a Series of Metal-Dielectric Interfaces by the Transient Thermoreflectance Technique," *ASME J. Heat Transfer*, **127**, pp. 315–322.
- Reddy, P., Castolino, K., and Majumdar, A., 2005, "Diffuse Mismatch Model of Thermal Boundary Conductance Using Exact Phonon Dispersion," *Appl. Phys. Lett.*, **87**, p. 211908.
- Phelan, P. E., 1998, "Application of Diffuse Mismatch Theory to the Prediction of Thermal Boundary Resistance in Thin-Film High- T_c Superconductors," *ASME J. Heat Transfer*, **120**, pp. 37–43.
- Majumdar, A., and Reddy, P., 2004, "Role of Electron-Phonon Coupling in Thermal Conductance of Metal-Nonmetal Interfaces," *Appl. Phys. Lett.*, **84**, pp. 4768–4770.
- Beechem, T. E., Graham, S., Hopkins, P. E., and Norris, P. M., 2007, "The Role of Interface Disorder on Thermal Boundary Conductance Using a Virtual Crystal Approach," *Appl. Phys. Lett.*, **90**, p. 054104.
- Prasher, R. S., and Phelan, P. E., 2001, "A Scattering-Mediated Acoustic Mismatch Model for the Prediction of Thermal Boundary Resistance," *ASME J. Heat Transfer*, **123**, pp. 105–112.
- Beechem, T., and Hopkins, P. E., 2009, "Predictions of Thermal Boundary Conductance for Systems of Disordered Solids and Interfaces," *J. Appl. Phys.*, **106**, p. 124301.
- Stoner, R. J., and Maris, H. J., 1993, "Kapitza Conductance and Heat Flow Between Solids at Temperatures From 50 to 300 K," *Phys. Rev. B*, **48**, pp. 16373–16387.
- Huberman, M. L., and Overhauser, A. W., 1994, "Electronic Kapitza Conductance at a Diamond-Pb Interface," *Phys. Rev. B*, **50**, pp. 2865–2873.
- Sergeev, A. V., 1998, "Electronic Kapitza Conductance Due To Inelastic Electron-Boundary Scattering," *Phys. Rev. B*, **58**, p. R10199.
- Sergeev, A. V., 1999, "Inelastic Electron-Boundary Scattering in Thin Films," *Physica B*, **263–264**, pp. 217–219.
- Chen, Y., Li, D., Yang, J., Wu, Y., Lukes, J., and Majumdar, A., 2004, "Molecular Dynamics Study of the Lattice Thermal Conductivity of Kr/Ar Superlattice Nanowires," *Physica B*, **349**, pp. 270–280.
- Stevens, R. J., Zhigilei, L. V., and Norris, P. M., 2007, "Effects of Temperature and Disorder on Thermal Boundary Conductance at Solid-Solid Interfaces: Nonequilibrium Molecular Dynamics Simulations," *Int. J. Heat Mass Transfer*, **50**, pp. 3977–3989.
- Kittel, C., 1996, *Introduction to Solid State Physics*, Wiley, New York.
- Hopkins, P. E., Salaway, R. N., Stevens, R. J., and Norris, P. M., 2007, "Temperature Dependent Thermal Boundary Conductance at Al/Al₂O₃ and Pt/Al₂O₃ Interfaces," *Int. J. Thermophys.*, **28**, pp. 947–957.
- Snyder, N. S., 1970, "Heat Transport Through Helium II: Kapitza Conductance," *Cryogenics*, **10**, pp. 89–95.
- Klemens, P. G., 1966, "Anharmonic Decay of Optical Phonons," *Phys. Rev.*, **148**, pp. 845–848.
- Norris, P. M., and Hopkins, P. E., 2009, "Examining Interfacial Diffuse Phonon Scattering Through Transient Thermoreflectance Measurements of Thermal Boundary Conductance," *ASME J. Heat Transfer*, **131**, p. 043207.
- Chen, G., 1998, "Thermal Conductivity and Ballistic-Phonon Transport in the Cross-Plane Direction of Superlattices," *Phys. Rev. B*, **57**, pp. 14958–14973.
- Dames, C., and Chen, G., 2004, "Theoretical Phonon Thermal Conductivity of Si/Ge Superlattice Nanowires," *J. Appl. Phys.*, **95**, pp. 682–693.
- Hopkins, P. E., and Norris, P. M., 2007, "Effects of Joint Vibrational States on Thermal Boundary Conductance," *Nanoscale Microscale Thermophys. Eng.*, **11**, pp. 247–257.
- Kosevich, Y. A., 1995, "Fluctuation Subharmonic and Multiharmonic Phonon Transmission and Kapitza Conductance Between Crystals With Very Different Vibrational Spectra," *Phys. Rev. B*, **52**, pp. 1017–1024.
- Hopkins, P. E., and Norris, P. M., 2009, "Relative Contributions of Inelastic and Elastic Diffuse Phonon Scattering to Thermal Boundary Conductance Across Solid Interfaces," *ASME J. Heat Transfer*, **131**, p. 022402.
- Hopkins, P. E., 2009, "Multiple Phonon Processes Contributing to Inelastic Scattering During Thermal Boundary Conductance at Solid Interfaces," *J. Appl. Phys.*, **106**, p. 013528.
- Chen, G., 2005, *Nanoscale Energy Transport and Conversion: A Parallel Treatment of Electrons, Molecules, Phonons, and Photons*, Oxford University Press, New York.
- Zhang, Z., 2007, *Nano/Microscale Heat Transfer*, McGraw-Hill, New York.
- Gray, D. E., 1972, *American Institute of Physics Handbook*, McGraw-Hill, New York.
- Touzelbaev, M. N., and Goodson, K. E., 1997, "Impact of Nucleation Density on Thermal Resistance Near Diamond-Substrate Boundaries," *J. Thermophys. Heat Transfer*, **11**, pp. 506–512.
- Duda, J. C., Beechem, T., Smoyer, J. L., Norris, P. M., and Hopkins, P. E., 2010, "The Role of Dispersion on Phononic Thermal Boundary Conductance," *J. Appl. Phys.*, **108**, p. 073515.
- Chen, Z., Jang, W., Bao, W., Lau, C. N., and Dames, C., 2009, "Thermal Contact Resistance Between Graphene and Silicon Dioxide," *Appl. Phys. Lett.*, **95**, p. 161910.
- Duda, J. C., Hopkins, P. E., Smoyer, J. L., Bauer, M. L., English, T. S., Saltonstall, C. B., and Norris, P. M., 2010, "On the Assumption of Detailed Balance in Prediction of Diffusive Transmission Probability During Interfacial Transport," *Nanoscale Microscale Thermophys. Eng.*, **14**, pp. 21–33.
- Vincenti, W. G., and Kruger, C. H., 2002, *Introduction to Physical Gas Dynamics*, Krieger, Malabar, FL.
- Majumdar, A., 1993, "Microscale Heat Conduction in Dielectric Thin Films," *ASME J. Heat Transfer*, **115**, pp. 7–16.
- Chen, G., 1997, "Size and Interface Effects on Thermal Conductivity of Superlattices and Periodic Thin-Film Structures," *ASME J. Heat Transfer*, **119**, pp. 220–229.
- Yang, R., and Chen, G., 2004, "Thermal Conductivity Modeling of Periodic Two-Dimensional Nanocomposites," *Phys. Rev. B*, **69**, p. 195316.
- Brockhouse, B. N., Arase, T., Caglioti, G., Rao, K. R., and Woods, A. D. B., 1962, "Crystal Dynamics of Lead. I. Dispersion Curves at 100 K," *Phys. Rev.*, **128**, pp. 1099–1111.
- Weber, W., 1977, "Atomic Bond Charge Model for the Phonons in Diamond, Si, Ge, and α -Sn," *Phys. Rev. B*, **15**, pp. 4789–4803.
- Turney, J. E., Mcgaughey, A. J. H., and Amon, C. H., 2009, "Assessing the Applicability of Quantum Corrections to Classical Thermal Conductivity Predictions," *Phys. Rev. B*, **79**, p. 224305.